

Vacancy-induced supersolidity of the second ^4He layer on a biphenylene carbon sheet

Jeonghwan Ahn^{*} and Yongkyung Kwon[†]*Department of Physics, Konkuk University, Seoul 05029, Korea*
 (Received 23 September 2022; revised 6 February 2023; accepted 6 March 2023; published 16 March 2023)

We have performed path-integral Monte Carlo calculations to investigate various quantum phases of ^4He layers adsorbed on a biphenylene sheet, a recently synthesized two-dimensional network of carbon atoms. Three different commensurate solid phases are identified in the first ^4He layer, which is found to be completed to a $C_{2/2}$ commensurate solid at an areal density of 0.119 \AA^{-2} . We have also found that the commensurate structure of the completed first layer allows second-layer ^4He atoms to constitute a stable commensurate $C_{2/3}$ structure at a total helium coverage of 0.199 \AA^{-2} . Furthermore, this second-layer commensurate structure is observed to be stable even with the formation of vacancies that are mobile to instigate the superfluid response at low temperatures. This unequivocally shows that vacancy-induced supersolidity can be realized in the second ^4He layer on biphenylene.

DOI: [10.1103/PhysRevB.107.094510](https://doi.org/10.1103/PhysRevB.107.094510)

I. INTRODUCTION

Supersolidity, a simultaneous manifestation of superfluid and crystalline orders, has drawn a great deal of interest since its possible existence was predicted a few decades ago for quantum crystal [1]. Especially, Kim and Chan's observation of period drops in torsional oscillator (TO) experiments [2,3] for bulk solid ^4He , which was originally interpreted to be a signal of nonclassical rotational inertia, intensified scientific pursuit of this new state of matter. However, this interpretation was later revisited in another TO experiment with more rigorous design [4] and the period drop was concluded to be due to stiffening of solid ^4He when cooled, which was first observed by Day and Beamish through their shear modulus measurements [5]. Although the controversy regarding the interpretation of TO experiments for bulk solid ^4He persisted, a series of theoretical studies predicted the existence of a supersolid phase for a bosonic model on a two-dimensional (2D) lattice [6–8]. In addition, there were some recent experimental reports of observing supersolid phenomena due to translational symmetry breaking in optically trapped Bose-Einstein condensates [9–11]. Concurrent with this development, efforts of searching for a supersolid phase in an extended quantum solid have been focused on ^4He atoms adsorbed on a carbon substrate, which form a quasi-2D quantum system in a layer-by-layer fashion to be a desirable platform for pursuit of this elusive state of matter.

^4He adlayers on graphite are known to display rich quantum phases as a result of appropriate interplay between ^4He -substrate and ^4He - ^4He interactions. Although various solid phases, both commensurate and incommensurate ones, were observed in the first ^4He layer [12–16], TO experiments of Crowell and Reppy [17] first revealed the superfluid response of the second ^4He layer on graphite. This, in com-

ination with the observations of anomalous heat-capacity peaks [18,19] that were interpreted to be melting signals of a second-layer commensurate solid, led to an early speculation of 2D supersolidity. Recently, based on their own TO experiments for the second ^4He layer, Nyekí *et al.* proposed a new quantum phase of intertwined superfluid and density wave order [20]. This spatially modulated superfluid phase was confirmed by more recent rigid two-frequency TO experiments of Choi *et al.* [21], which also led them to suggest a supersolid phase at higher helium coverages. However, there is no direct experimental evidence for a second-layer commensurate solid phase for ^4He on graphite, whose existence was conjectured only indirectly through heat-capacity measurements. In addition, there is currently no consensus on this issue among different theoretical studies. A series of path-integral Monte Carlo (PIMC) calculations showed that no commensurate solid structure was stable in the second ^4He layer on graphite or graphene [14–16]. Two recent diffusion Monte Carlo studies reported contradictory predictions; no commensurate solid phase was concluded in one study [22] to be stable in the second 4 layer whereas the other predicted that a $7/12$ commensurate solid would be stable with accompanying substantial superfluid response [23].

Various types of 2D carbon networks other than graphene have been recently proposed and pursued because of their potential applications for all carbon electronics as well as intriguing electronic and mechanical properties. Some of them, such as γ graphyne [24], holey graphyne [25], and γ graphdiyne [26], were successfully synthesized as extended forms of atomically thin carbon sheets. Because of different pore sizes and lattice symmetries, ^4He atoms on these new carbon sheets are expected to exhibit more complex and diverse quantum phases than ^4He on graphite. Among them, we here consider a biphenylene sheet, which consists of eight-, six-, and four-membered carbon rings (see Fig. 1) as a substrate for ^4He atoms. This 2D network of sp^2 -bonded carbon atoms with rectangular symmetry was recently synthesized in an extended form through two-step interpolymer dehydrofluorination polymerization process [27]. Through PIMC

^{*}Present address: Materials Science and Technology Division, Oak Ridge National Laboratory, Oak Ridge, Tennessee 37831, United States.

[†]ykwon@konkuk.ac.kr

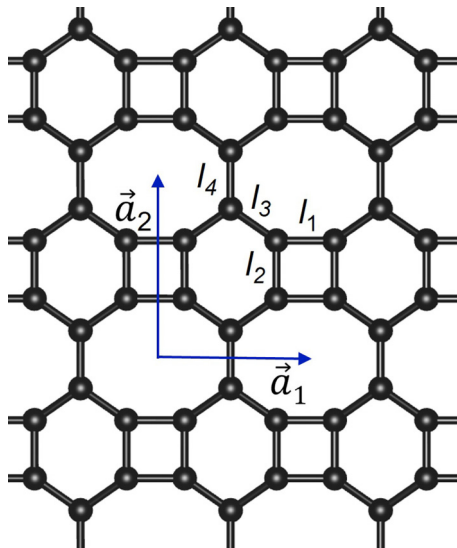


FIG. 1. An atomic structure of a biphenylene sheet consisting of eight-, six-, and four-membered carbon rings. The blue arrows \vec{a}_1 and \vec{a}_2 represent its primitive vectors whose magnitudes are 3.73 and 4.48 Å, respectively. There are four different bond lengths in the biphenylene sheet; $l_1 = 1.445$, $l_2 = 1.447$, $l_3 = 1.397$, and $l_4 = 1.434$ Å.

calculations, we discover three different commensurate solid phases in a ^4He monolayer on biphenylene. In addition, the first ^4He layer is found to be completed as a $C_{2/2}$ commensurate solid at an areal density of 0.119 \AA^{-2} . More interestingly, we find that a stable commensurate solid structure is developed in the second ^4He layer without disrupting the underlying first-layer $C_{2/2}$ structure. This second-layer commensurate solid structure is found to be stable with the formation of mobile vacancies, leading to finite superfluid response at low temperatures. This suggests that the second ^4He layer on biphenylene can exhibit a vacancy-induced supersolid phase.

II. METHODOLOGY

In this paper, the ^4He -biphenylene interaction is described by a pairwise sum of isotropic ^4He -C interatomic potentials proposed by Carlos and Cole [28] and Cole and Klein [29] to fit ^4He -scattering data on graphite. A well-known potential of Aziz *et al.* [30] is used for the ^4He - ^4He interaction. In the discrete path-integral representation, a thermal density matrix at a low-temperature T is expressed by a convolution of M high-temperature density matrices with an imaginary time-step $\tau = (Mk_B T)^{-1}$. We use ^4He - ^4He and ^4He -C pair potentials to derive pair product forms of exact two-body density matrices at a high-temperature MT [31,32] where Catoms are treated to be immobile with infinite mass and to provide only external potentials for ^4He atoms. For this, the time step of $\tau^{-1}/k_B = 40 \text{ K}$ turns out to provide an accurate description for the interaction between a ^4He atom and the sp^2 -bonded carbon sheet as well as the ^4He - ^4He interaction (see Sec. I of the Supplemental Material [33]), which was also confirmed in our previous PIMC studies for ^4He on other carbon substrates, such as graphene [15] and graphyne [34].

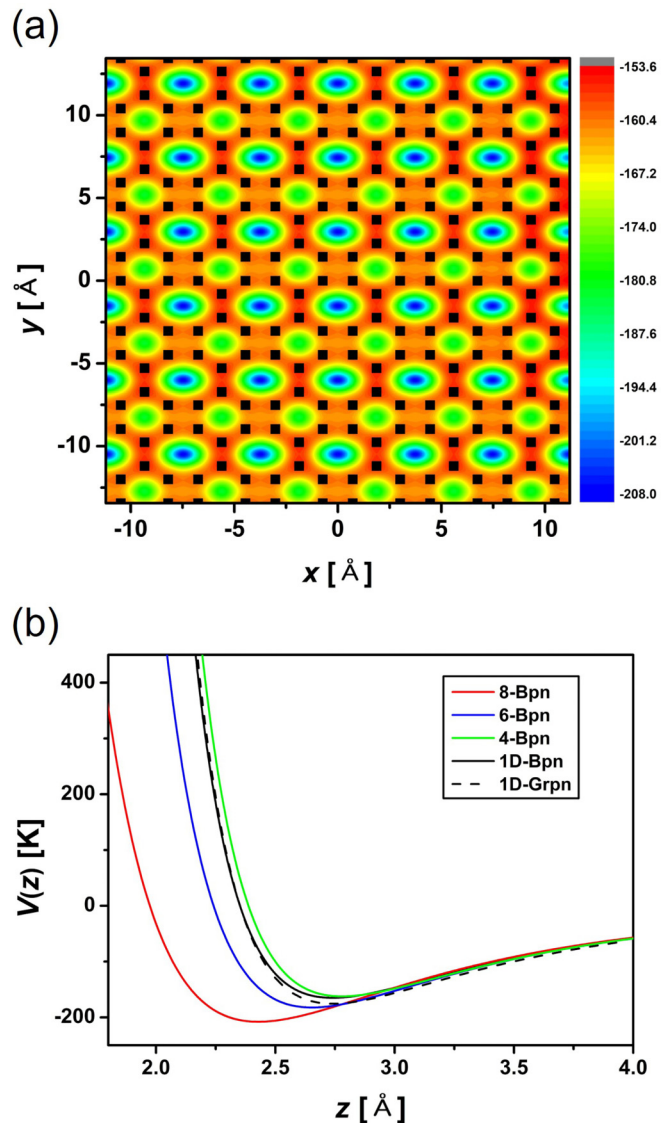


FIG. 2. (a) A contour plot of the minimum ^4He -biphenylene potential, $V_{\min}(x, y)$, above each point (x, y) on biphenylene and (b) ^4He -biphenylene potentials as functions of the vertical distance z from the carbon surface along different symmetry directions. Although the red, the blue, and the green solid lines in (b) correspond to the vertical direction passing through an octagon, a hexagon, and a rectangle center, respectively, the black solid (dashed) line represents the laterally averaged one-dimensional (1D) ^4He -biphenylene (^4He -graphene) potential as a function of the vertical distance.

The multilevel Metropolis algorithm described in Ref. [31] has been employed to sample the imaginary time paths as well as the permutations among ^4He atoms. To minimize finite-size effects, we apply periodic boundary conditions along the lateral directions, and no boundary condition is applied for the direction perpendicular to the biphenylene surface.

III. RESULTS

We first examine the ^4He -biphenylene interaction made of empirical ^4He -C pair potentials to find preferred adsorption sites for ^4He atoms. A contour plot of the minimum

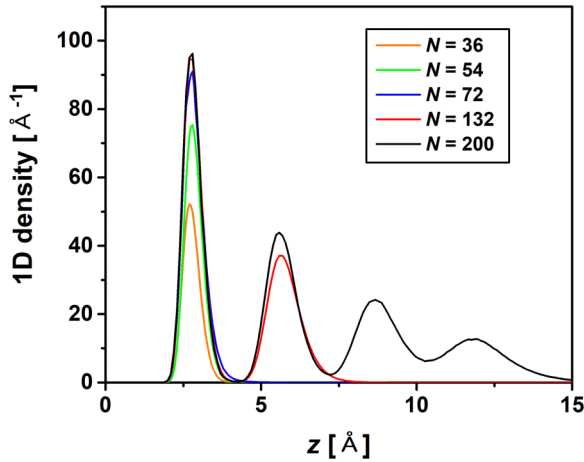


FIG. 3. One-dimensional density distributions of ^4He atoms as functions of the vertical distance z from a biphenylene sheet. Here, N represents the number of ^4He atoms per 6×6 simulation cell whose dimensions are $22.40 \times 26.89 \text{ \AA}^2$. The computations were performed at a temperature of 0.5 K.

^4He -biphenylene potential-energy $V_{\min}(x, y)$ above each point (x, y) on a biphenylene surface is presented in Fig. 2(a), which reveals that there are two ^4He adsorption sites per rectangular unit cell of biphenylene with an octagon center being the most stable one. Figure 2(b) shows the ^4He -biphenylene potential energies, along different symmetry directions as functions of the vertical distance from the biphenylene surface. Here one can see that the laterally averaged 1D ^4He -biphenylene potential curve is very close to the corresponding ^4He -graphene potential, which indicates that a biphenylene substrate provides as strong a ^4He adsorption potential as the ^4He -graphene interaction. This is understood to reflect that the areal density of carbon atoms in a biphenylene sheet is comparable to that of graphene.

In this paper, we consider ^4He adsorption only on one side of a biphenylene sheet. Figure 3 presents 1D ^4He density distributions computed at a temperature of 0.5 K as

functions of the vertical coordinate z from a biphenylene sheet. Here, N represents the number of ^4He adatoms per 6×6 simulation cell whose dimensions are $22.40 \times 26.89 \text{ \AA}^2$. Zero ^4He density for $z < 0$ indicates that a biphenylene sheet is impermeable to ^4He atoms, such as graphene. One can see the development of multiple distinct density peaks in Fig. 3 as the helium coverage increases beyond $N = 72$, which confirms a layer-by-layer growth of ^4He atoms on biphenylene as on graphite or graphene [14,15]. Furthermore, the first density peak located at $z \sim 2.8 \text{ \AA}$ is observed to change little for $N \geq 72$, suggesting that the first layer is completed at $N = 72$ which corresponds to an areal density of 0.119 \AA^{-2} . This completion density is nearly identical to the experimental values of $0.115\text{--}0.121 \text{ \AA}^{-2}$ for the completion density of the first ^4He layer on graphite [12,19,20,35]. This can be understood by the fact that biphenylene and graphene substrates provide the adsorption potentials of similar strength for ^4He atoms as seen in Fig. 2(b). Considering that there are 72 adsorption sites in total, 36 octagon centers plus 36 hexagon centers in our 6×6 simulation cell [see Fig. 2(a)], one would conjecture that each of these adsorption sites accommodates a single ^4He atom to form a commensurate solid structure with $2/2$ filling at the first layer completion of $N = 72$. Note that our PIMC simulations started from configurations where all ^4He atoms were randomly distributed at the distances of $7\text{--}9 \text{ \AA}$ from a biphenylene sheet. This is understood to warrant that the structural features of the first two ^4He layers revealed in this paper were not affected by initial configurations.

For a detailed analysis of the ^4He monolayer adsorbed on a biphenylene sheet, we computed 2D density distributions along the lateral directions at various ^4He coverages. From this, we could identify three different commensurate solids in the ^4He monolayer at areal densities of 0.060, 0.090, and 0.119 \AA^{-2} , whose 2D density distributions are shown in Fig. 4. Although each distinct peak in Fig. 4 corresponds to a single occupancy of a ^4He atom, the white rectangles represent common unit cells of these ^4He lattices and the underlying biphenylene lattice, whose existence signifies their commensurability. At an areal density of 0.060 \AA^{-2} , all ^4He atoms occupy the octagon centers and constitute a

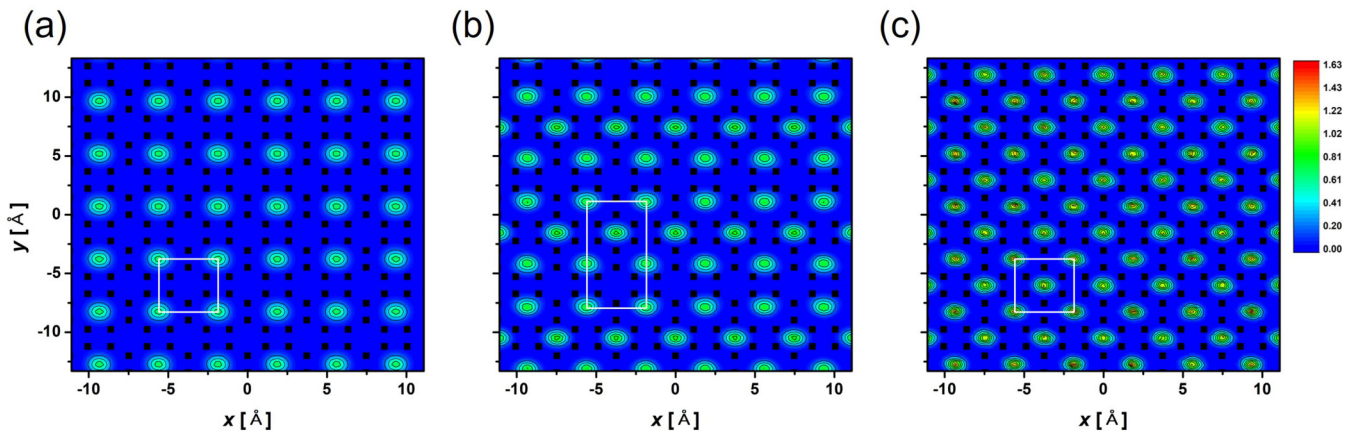


FIG. 4. Two-dimensional density distributions of the first-layer ^4He atoms adsorbed on biphenylene at areal densities of (a) 0.060 \AA^{-2} , (b) 0.090 \AA^{-2} , and (c) 0.119 \AA^{-2} . The black dots represent the positions of the carbon atoms of biphenylene. The computations were performed at a temperature of 0.5 K. The rectangle enclosed by white lines in (a)–(c) represents a common unit cell of each commensurate structure with the underlying biphenylene lattice. All contour plots are in the same color scale denoted by the color bar on the right-hand side.

commensurate solid structure characterized by the rectangular lattice shown in Fig. 4(a), reflecting the symmetry of the underlying biphenylene substrate. Its common unit cell with the biphenylene lattice (the white rectangle in the figure) includes two adsorption sites; one at the octagon center and another at the hexagon center. With only one of these two sites being occupied by a ^4He atom, this ^4He solid is referred to as a $1/2$ commensurate structure, or a $C_{1/2}$ structure with respect to the underlying biphenylene lattice. In Fig. 4(b), one can see another commensurate structure of $C_{3/4}$ where three out of four adsorption sites in a common unit cell are occupied by ^4He atoms. As can be seen, this $C_{3/4}$ structure shows a rectangular arrangement of rhombic rings of ^4He atoms. We note that the first-layer ^4He atoms adsorbed on 6,6,12-graphyne share the same crystalline ordering with this $C_{3/4}$ structure (see Fig. 3 of Ref. [36]). Furthermore, ^4He atoms are found to form a $C_{2/2}$ commensurate structure at the first-layer completion density of 0.119 \AA^{-2} where both of the two adsorption sites in the common unit cell are occupied by ^4He atoms as displayed in Fig. 4(c). This confirms a conjecture drawn from 1D density analysis that the completed first ^4He layer on biphenylene is in a $C_{2/2}$ commensurate solid phase, unlike the first ^4He layer on graphite, which is completed to an incommensurate triangular solid [12,18]. This $C_{2/2}$ solid, where ^4He atoms constitute a centered-rectangular lattice, is the densest first-layer commensurate structure among the ones reported so far to form on various carbon substrates. We note that the translational invariance of the biphenylene lattice is broken along the y direction in the $C_{2/3}$ solid, whereas, it is preserved in the $C_{1/2}$ and the $C_{2/2}$ solids. As seen in Fig. 2 of the Supplemental Material [33], the formation of these first-layer commensurate structures was not affected by finite sizes of our simulation cells.

As the ^4He coverage increases beyond an areal density of 0.119 \AA^{-2} , the first-layer completion density, the second layer develops without disrupting the first-layer $C_{2/2}$ structure as demonstrated in 1D density distributions of Fig. 3. When the total helium coverage becomes 0.199 \AA^{-2} , the second-layer ^4He atoms are found to form an elongated honeycomb structure, a centered-rectangular lattice with a two-atom basis, that is commensurate with the underlying first-layer $C_{2/2}$ solid as shown in Fig. 5(a). A common unit cell enclosed by yellow lines in the figure contains two second-layer atoms and three first-layer ones. Thus, this second-layer ^4He solid corresponds to a $C_{2/3}$ commensurate structure with respect to the first-layer $C_{2/2}$ solid. Considering that these second-layer ^4He atoms are located above saddle points, not adsorption sites, on a biphenylene surface (every adsorption site is occupied by a first-layer ^4He atom), one can say that their solidification is mostly determined by the ^4He - ^4He interaction and the ^4He -biphenylene interaction has only indirect effects. However, the completion of the first ^4He layer to a commensurate solid on biphenylene is understood to play a critical role in stabilizing a second-layer commensurate structure as noted in our previous PIMC study for the ^4He -graphite system [16]. Interestingly, the total helium coverage of 0.199 \AA^{-2} for the second-layer $C_{2/3}$ solid on top of the first-layer $C_{2/2}$ solid is very close to the helium coverage of 0.197 \AA^{-2} where anomalous heat-capacity peaks were observed for ^4He on graphite [18,19].

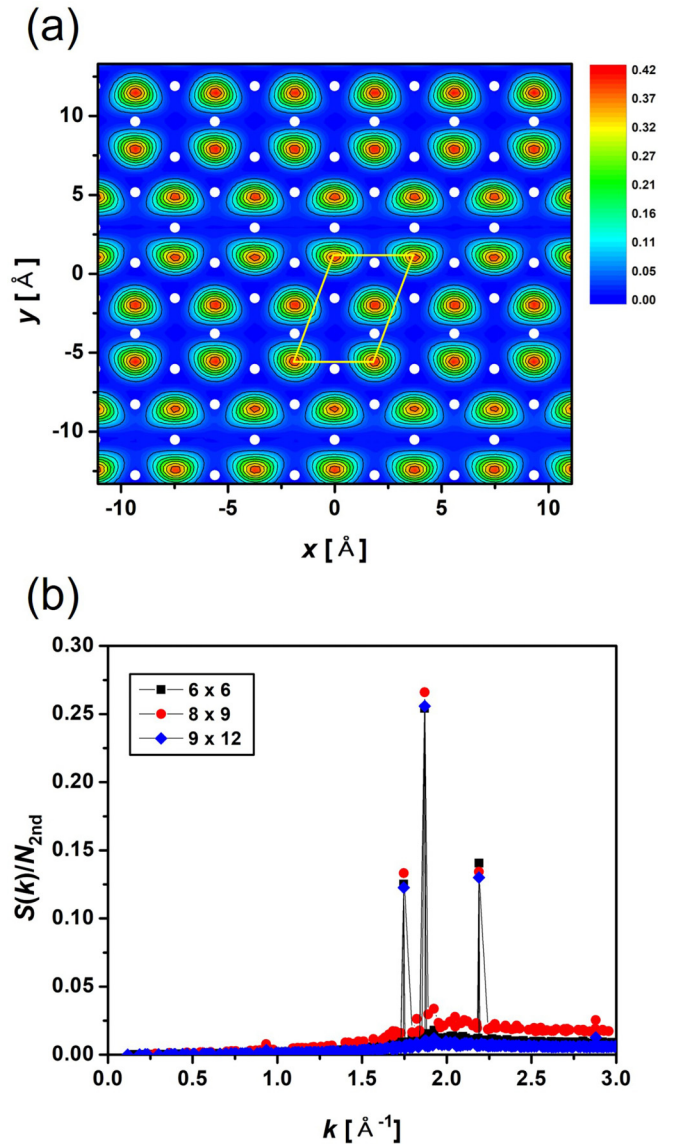


FIG. 5. (a) Two-dimensional density distribution of the second-layer ^4He atoms at a total helium coverage of 0.199 \AA^{-2} and (b) their 2D static structure factors divided by the number of ^4He atoms as a function of wave-vector k for different sizes of the simulation cell, namely, the 6×6 , the 8×9 , and the 9×12 cells. The white dots in (a) represent the peak positions of the first-layer ^4He density distribution, whereas, the yellow parallelogram denotes a common unit cell of the first and the second layers ^4He lattice. The computations were performed at a temperature of 0.5 K , and statistical errors of the data shown in (b) are smaller than the symbol sizes.

For further analysis for the crystalline ordering of the second-layer ^4He atoms, we computed static structure factors as functions of the magnitude of the wave vectors, which are presented in Fig. 5(b). As can be seen, the structure factor of the second-layer $C_{2/3}$ solid is featured by three major peaks at $k = 1.7466, 1.8693,$ and 2.1903 \AA^{-1} , which reflects its rectangular symmetry. In addition, Fig. 5(b) shows that there are little differences between the structure factors computed with the simulation cells of different sizes. From this, we conclude that the manifestation of the second-layer $C_{2/3}$ commensurate solid is not affected by finite sizes of our simulation cells.

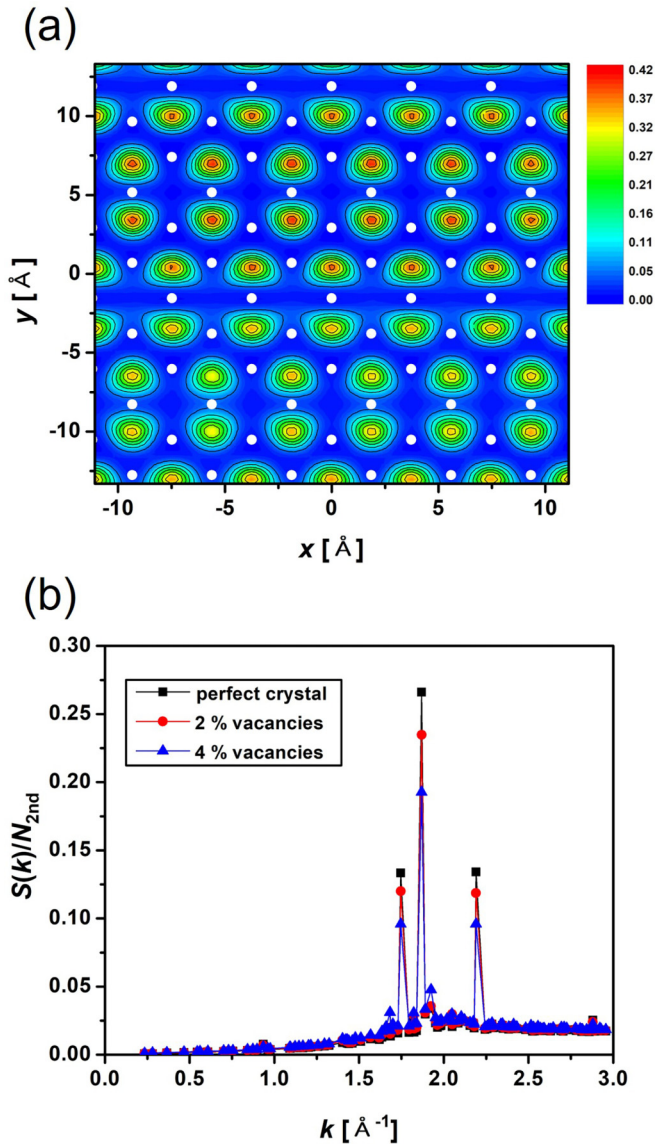


FIG. 6. (a) Two-dimensional density distribution of the second-layer ^4He atoms at a total helium coverage of 0.198 \AA^{-2} (vacancy concentration of 2% in a second-layer $C_{2/3}$ solid) and (b) their 2D static structure factors divided by the number of ^4He atoms as functions of wave-vector k for different vacancy concentrations. The white dots in (a) represent the peak positions of the first-layer ^4He density distribution. The computations were performed at a temperature of 0.5 K with the 6×6 simulation cell and statistical errors of the data shown in (b) are smaller than the symbol sizes.

We now examine the stability of this second-layer $C_{2/3}$ structure against vacancy formation. Figure 6(a) presents 2D density distribution of the second layer involving one less ^4He atom per 6×6 simulation cell than the perfect $C_{2/3}$ solid, which corresponds to a vacancy concentration of about 2%. One can see the same crystalline structure, including the same number of density peaks as the one for the perfect $C_{2/3}$ solid of Fig. 5(a). This indicates that vacancies created in the second-layer $C_{2/3}$ solid are uniformly distributed and are mobile over the lattice sites through frequent hopping of ^4He atoms from occupied sites to vacant ones. The corresponding structure

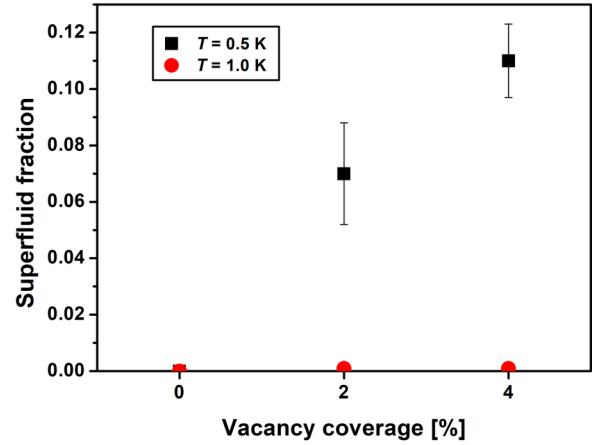


FIG. 7. Superfluid fractions of ^4He atoms constituting the second-layer $C_{2/3}$ solid at different vacancy concentrations. The computations were performed at two different temperatures of 0.5 K (black squares) and 1.0 K (red circles) with the 6×6 simulation cell.

factor peaks, along with the ones for a vacancy concentration of 4%, are seen in Fig. 6(b) to be located at the same k vectors, albeit with reduced peak heights as in the case of the $C_{2/3}$ solid without vacancy. This suggests that structural features of the second-layer $C_{2/3}$ solid are preserved with the formation of some vacancies.

Finally, we computed the superfluid response of the second-layer $C_{2/3}$ solid with the winding number estimator whose detailed description was presented in Ref. [31]. Figure 7 shows superfluid fractions of the second-layer $C_{2/3}$ solid at different vacancy concentrations, which were computed at temperatures of 0.5 and 1.0 K. No winding paths (no superfluidity) were sampled in a perfect $C_{2/3}$ solid at both temperatures. Superfluid fractions were estimated to be 0.07(2) and 0.11(1) at a temperature of 0.5 K for vacancy concentrations of 2% and 4%, respectively, whereas their superfluid responses are seen to be negligible, regardless of the vacancy concentration at 1.0 K. This, along with preservation of the crystalline order against vacancy formation, leads us to conclude that vacancy-induced supersolidity is manifested in the second-layer $C_{2/3}$ solid at a temperature of 0.5 K. On the other hand, we did not observe any sign of the superfluid response, regardless of vacancy concentrations, in the first-layer commensurate solids (see Sec. III of the Supplemental Material [33] for further details), suggesting that supersolidity can be realized only in the second ^4He layer.

IV. CONCLUSION

In conclusion, our PIMC study has revealed that a supersolid phase, a coexistence of crystalline and superfluid order, can be realized in the second ^4He layer on biphenylene. Three different commensurate solid structures of $C_{1/2}$, $C_{3/4}$, and $C_{2/2}$ are found in the first ^4He layer on biphenylene, all of which possess rectangular symmetry to reflect the symmetry of the biphenylene sheet. The first layer is completed to the $C_{2/2}$ structure at a helium coverage of 0.119 \AA^{-2} , which is understood to be a key factor to stabilize the second-layer $C_{2/3}$ commensurate solid. The crystalline order of the second-layer

$C_{2/3}$ solid is preserved in the presence of vacancy defects, which are observed to be mobile and to induce finite superfluid response. We also note that because of the rectangular symmetry of the underlying first layer, density modulations of the second-layer ^4He superfluid on biphenylene is expected to have different features from hexatic density modulations identified recently for ^4He on graphite [19–21,23]. This could result in unique intertwining characteristic between superfluid and density wave order for ^4He on biphenylene. In this regard, an experimentally accessible ^4He -biphenylene system should be considered an original platform to seek novel quantum phases, including long sought-after supersolidity, which calls

for experimental confirmation as well as further theoretical investigation.

ACKNOWLEDGMENTS

Y.K. was supported by the Basic Science Research Program (Grant No. NRF-2018R1D1A1B07042443) through the National Research Foundation of Korea funded by the Ministry of Education. We also acknowledge the support from the Supercomputing Center/Korea Institute of Science and Technology Information with supercomputing resources including technical support (Grant No. KSC-2021-CRE-0501).

-
- [1] A. F. Andreev and I. M. Lifshitz, *Sov. Phys. JETP* **29**, 1107 (1969).
- [2] E. Kim and M. H. Chan, *Science* **305**, 1941 (2004).
- [3] E. Kim and M. H.-W. Chan, *Nature (London)* **427**, 225 (2004).
- [4] D. Y. Kim and M. H. W. Chan, *Phys. Rev. Lett.* **109**, 155301 (2012).
- [5] J. Day and J. Beamish, *Nature (London)* **450**, 853 (2007).
- [6] M. Boninsegni and N. Prokofev, *Phys. Rev. Lett.* **95**, 237204 (2005).
- [7] S. Wessel and M. Troyer, *Phys. Rev. Lett.* **95**, 127205 (2005).
- [8] L. Dang, M. Boninsegni, and L. Pollet, *Phys. Rev. B* **78**, 132512 (2008).
- [9] J. Léonard, A. Morales, P. Zupancic, T. Esslinger, and T. Donner, *Nature (London)* **543**, 87 (2017).
- [10] J.-R. Li, J. Lee, W. Huang, S. Burchesky, B. Shteynas, F. Ç. Top, A. O. Jamison, and W. Ketterle, *Nature (London)* **543**, 91 (2017).
- [11] L. Chomaz, D. Petter, P. Ilzhöfer, G. Natale, A. Trautmann, C. Politi, G. Durastante, R. M. W. van Bijnen, A. Patscheider, M. Sohmen, M. J. Mark, and F. Ferlaino, *Phys. Rev. X* **9**, 021012 (2019).
- [12] D. S. Greywall and P. A. Busch, *Phys. Rev. Lett.* **67**, 3535 (1991).
- [13] M. E. Pierce and E. Manousakis, *Phys. Rev. Lett.* **83**, 5314 (1999).
- [14] P. Corboz, M. Boninsegni, L. Pollet, and M. Troyer, *Phys. Rev. B* **78**, 245414 (2008).
- [15] Y. Kwon and D. M. Ceperley, *Phys. Rev. B* **85**, 224501 (2012).
- [16] J. Ahn, H. Lee, and Y. Kwon, *Phys. Rev. B* **93**, 064511 (2016).
- [17] P. A. Crowell and J. D. Reppy, *Phys. Rev. B* **53**, 2701 (1996).
- [18] D. S. Greywall, *Phys. Rev. B* **47**, 309 (1993).
- [19] S. Nakamura, K. Matsui, T. Matsui, and H. Fukuyama, *Phys. Rev. B* **94**, 180501(R) (2016).
- [20] J. Nyéki, A. Phillis, A. Ho, D. Lee, P. Coleman, J. Parpia, B. Cowan, and J. Saunders, *Nat. Phys.* **13**, 455 (2017).
- [21] J. Choi, A. A. Zadorozhko, J. Choi, and E. Kim, *Phys. Rev. Lett.* **127**, 135301 (2021).
- [22] S. Moroni and M. Boninsegni, *Phys. Rev. B* **99**, 195441 (2019).
- [23] M. C. Gordillo and J. Boronat, *Phys. Rev. Lett.* **124**, 205301 (2020).
- [24] Y. Hu, C. Wu, Q. Pan, Y. Jin, R. Lyu, V. Martinez, S. Huang, J. Wu, L. J. Wayment, N. A. Clark *et al.*, *Nat. Synth.* **1**, 449 (2022).
- [25] X. Liu, S. M. Cho, S. Lin, Z. Chen, W. Choi, Y.-M. Kim, E. Yun, E. H. Baek, and H. Lee, *Matter* **5**, 2306 (2022).
- [26] G. Li, Y. Li, H. Liu, Y. Guo, Y. Li, and D. Zhu, *Chem. Commun.* **46**, 3256 (2010).
- [27] Q. Fan, L. Yan, M. W. Tripp, O. Krejčí, S. Dimosthenous, S. R. Kachel, M. Chen, A. S. Foster, U. Koert, P. Liljeroth *et al.*, *Science* **372**, 852 (2021).
- [28] W. E. Carlos and M. W. Cole, *Surf. Sci.* **91**, 339 (1980).
- [29] M. W. Cole and J. R. Klein, *Surf. Sci.* **124**, 547 (1983).
- [30] R. A. Aziz, M. Slaman, A. Koide, A. Allnatt, and W. J. Meath, *Mol. Phys.* **77**, 321 (1992).
- [31] D. M. Ceperley, *Rev. Mod. Phys.* **67**, 279 (1995).
- [32] R. Zillich, F. Paesani, Y. Kwon, and K. Whaley, *J. Chem. Phys.* **123**, 114301 (2005).
- [33] See Supplemental Material at <http://link.aps.org/supplemental/10.1103/PhysRevB.107.094510> for details of time-step convergence, finite-size effect, and vacancy formation in the first ^4He layer.
- [34] J. Ahn, H. Lee, and Y. Kwon, *Phys. Rev. B* **90**, 075433 (2014).
- [35] M. Bretz, J. Dash, D. Hickernell, E. McLean, and O. Vilches, *Phys. Rev. A* **8**, 1589 (1973).
- [36] J. Ahn, M. You, G. Lee, T. Volkoff, and Y. Kwon, *Phys. Rev. B* **99**, 024113 (2019).